Characterization of collector optic material samples before and after exposure in laser produced plasma and discharge produced plasma extreme ultraviolet sources

Huatan Qiu
Darren A. Alman
Keith C. Thompson
Joshua B. Spencer
Erik L. Antonsen
Brian E. Jurczyk
D. N. Ruzic
University of Illinois at Urbana-Champaign
Department of Nuclear, Plasma and Radiological Engineering
103 S.Goodwin Avenue, 214 NEL
Urbana, Illinois 61801
E-mail: hqiu@uiuc.edu

Tim P. Spila
University of Illinois at Urbana-Champaign
Center for Microanalysis of Materials
Urbana, Illinois 61801

Abstract. The University of Illinois at Urbana-Champaign (UIUC) and several national laboratories are collaborating on an effort to characterize Xe plasma source exposure effects on extreme ultraviolet (EUV) collector optics. A series of mirror samples provided by SEMATECH were exposed for 10 million shots in an Xtreme Technologies XTS 13-35 commercial EUV discharge produced plasma (DPP) source at UIUC and 500,000 shots at the high-power TRW laser produced plasma (LPP) source at Sandia National Laboratory, Livermore (SNLL). Results for both pre- and post-exposure material characterization are presented for samples exposed in both facilities. Surface analysis performed at the Center for Microanalysis of Materials at UIUC investigates mirror degradation mechanisms by measuring changes in surface roughness, texture, and grain sizes as well as analysis of implantation of energetic ions, Xe diffusion, and mixing of multilayers. Materials characterization on samples removed after varying exposure times in the XTS source identify the onset of different degradation mechanisms within each sample over 1 million to 10 million shots. Results for DPP-exposed samples for 10 million shots in the XCEED (Xtreme Commercial EUV Emission Diagnostic) experiment show that samples are eroded and that the surface is roughened with little change to the texture. Atomic force microscopy (AFM) results show an increase in roughness by a factor of 2 to 6 times, with two exceptions. This is confirmed by x-ray reflectivity (XRR) data, which shows similar roughening characteristics and also confirms the smoothening of two samples. Scanning electron microscopy (SEM) pictures showed that erosion is from 5 to 54 nm, depending on the sample material and angle of incidence for debris ions. Finally, microanalysis of the exposed samples indicates that electrode material is implanted at varying depths in the samples. The erosion mechanism is explored using a spherical energy sector analyzer (ESA) to measure fast ion species and their energy spectra. Energy spectra for ions derived from various chamber sources are measured as a function of the argon flow rate and angle from the centerline of the pinch. Results show creation of high-energy ions (up to E=13 keV). Species noted include ions of Xe, Ar (a buffer gas), and various materials from the electrodes and debris tool. The bulk of fast ion ejection from the pinch includes Xe^{+}, which maximizes at ~8 keV, followed by Xe^{2+}, which maximizes at ~5 keV. Data from samples analysis and ESA measurements combined indicate mechanism and effect for debris-optic interactions and detail the effectiveness of the current debris mitigation schemes. [DOI: 10.1117/1.2243082]

Subject terms: collector optics; EUV; laser produced plasma; discharge produced plasma; erosion; debris mitigation.

Paper 05052R received Jul. 21, 2005; revised manuscript received Jan. 20, 2006; accepted for publication Feb. 16, 2006; published online Aug. 16, 2006. This paper is a revision of a paper presented at the SPIE Conference on Emerging Lithographic Technologies IX, Mar. 2005, San Jose, California. The paper presented there appears (unrefereed) in SPIE Proceedings Vol. 5751.

1 Introduction

This paper reports on part of the Collector Lifetime and Erosion Project at the University of Illinois at Urbana-Champaign (UIUC),[1–3] sponsored by SEMATECH and operated in cooperation with Intel Corporation and Xtreme Technologies GmbH.[4,5] The purpose of this project is to examine the effects of ion debris interaction with the primary collector optic in commercial EUV sources to ascer-

1537-1646/2006/$22.00 © 2006 SPIE

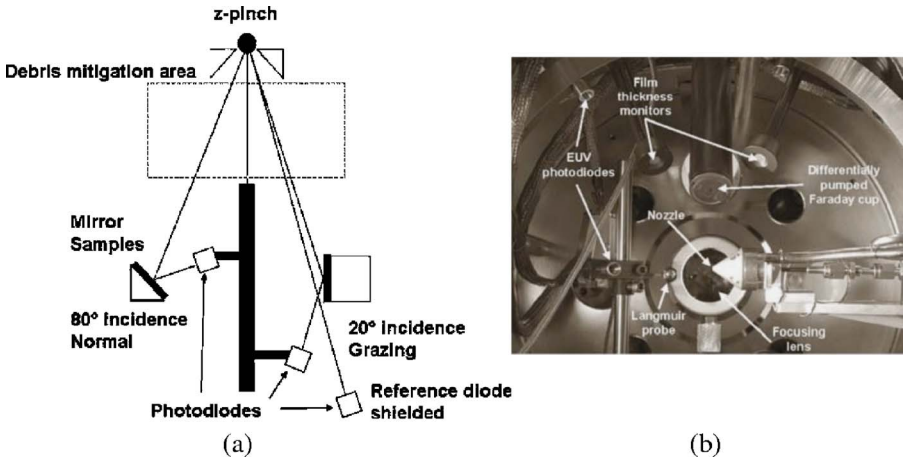

Fig. 1 Schematic of EUV exposure setup and working process, (a) DPP at UIUC. (Ref. 11), (b) LPP at SNLL (Ref. 6).

tain the fundamental erosion processes and critical lifetime issues facing high-volume manufacturing (HVM) for EUV lithography. This paper covers the comparative surface analysis between optically exposed samples at the Sandia National Laboratory, Livermore, (SNLL) laser produced plasma (LPP) experimental facility[6,7] and the UIUC discharge produced plasma (DPP) experimental facility.[8–11]

Film with a high reflectivity at 13.5 nm (the wavelength to be used for EUV lithography) and a high durability against erosion is needed to be the collector mirror in EUV applications. Based on the preceding criteria, seven samples are investigated consisting of one Si/Mo multilayer mirror (MLM) and six single material films of thickness ~200 nm deposited on Si substrates. The multilayer, named ML1, is optimized for 5-deg operation with 50 bilayer pairs with a period thickness of 4.17 nm Si and 2.78 nm Mo, and has a 2.3 nm Ru capping layer.[12] The six single films are Au, C, Mo, Pd, Ru, and Si. The ML1 and single films are all prepared using DC magnetron sputtering technique by Lawrence Livermore National Laboratory.[12,13]

The samples were exposed to 500,000 shots in the Engineering Test Stand (ETS) LPP Xe source at SNLL and to 10 million shots in a DPP Xe source at UIUC. The detailed experimental setup and conditions are discussed in Sec. 2. Surface characterization for both pre- and post-exposure in both facilities are performed to investigate mirror degradation mechanisms by measuring changes in surface roughness, texture, and grain sizes, as well as erosion and debris mitigation scheme, discussed in detail in Sec. 3.

2 Experiment Setup

The Xtreme[4] Commercial EUV Emission Diagnostic (XCEED) experiment is designed to investigate characterization of the DPP source and the debris fields emitted by the DPP, along with optical mirror exposure to the pinch plasma. XCEED experimental efforts are performed toward characterizing a commercial-scale DPP EUV source, including fast ion debris, debris mitigation techniques, methods to mitigate damage to collector mirrors, and exploring the characteristics and the erosive effects on the collector mirror surfaces after the DPP EUV exposures, by microanalysis measurements using atomic force microscopy (AFM), auger electron spectroscopy (AES), x-ray diffraction (XRD)/x-ray reflectivity (XRR), x-ray photoelectron spectroscopy (XPS), and scanning electron microscopy (SEM) techniques. The former experiments are detailed elsewhere,[11] and the latter are presented in this paper.

The XCEED DPP source creates a Xe z-pinch for the generation of 13.5-nm EUV light, which is characterized though a control photodiode. The DPP EUV exposure setup and working process[11] is shown in Fig. 1(a). The chamber allows characterization of optic samples at varying exposure times for normal and grazing incidence reflection angles.[9–11] All DPP mirror samples discussed here are placed 56 cm from pinch and exposed for 10 million pulses (~11 h exposure) with debris mitigation present. Au, C, Mo, Si, and ML1 are exposed at normal incidence (mirror plane is ~80 deg to the incoming light vector), while Pd and Ru are exposed at ~ 20-deg grazing incidence. The DPP exposure is operated at 256-Hz pinch frequency with 35 W over 2π steradian output EUV light (2% bandwidth) power with a conversion efficiency (CE) of 0.55%. The ellipsoid pinch geometry is ~1.5 mm × 0.5 mm. A foil trap-based debris mitigation tool with Ar buffer gas curtain,[14] which is similar to a collimator consisting of flat metal pieces placed with their normal direction perpendicular to the light path, is applied radially to reduce particle transfer from the pinch to the collector optics. Furthermore, an Ar buffer gas curtain flows through the debris tool at a high flow rate to enhance the scattering possibility for ejected particles from the pinch plasma. The chamber pressure during operation is 14 mTorr with 82 sccm Xe feed gas and the Ar buffer gas.

The LPP EUV exposure setup[6] is shown in Fig. 1(b). The collector mirrors are exposed in normal position at 10 to 17 cm from the source. A high-power TRW Nd:YAG laser is used to excite the LPP by producing 300 mJ pulses (4-ns pulselength) of 1.06-μm wavelength at 1667 pulses per second (500 W average power) with a CE of 0.30%. The nozzle is used to produce a stable 30-μm diameter Xe filament jet at a flow rate of 1050 sccm. The corresponding operation pressure is 3.6 mTorr. There is no debris mitigation tool at present. Only 500,000 shots (~5 min exposure) is performed because of problems with the Xe filament nozzle.

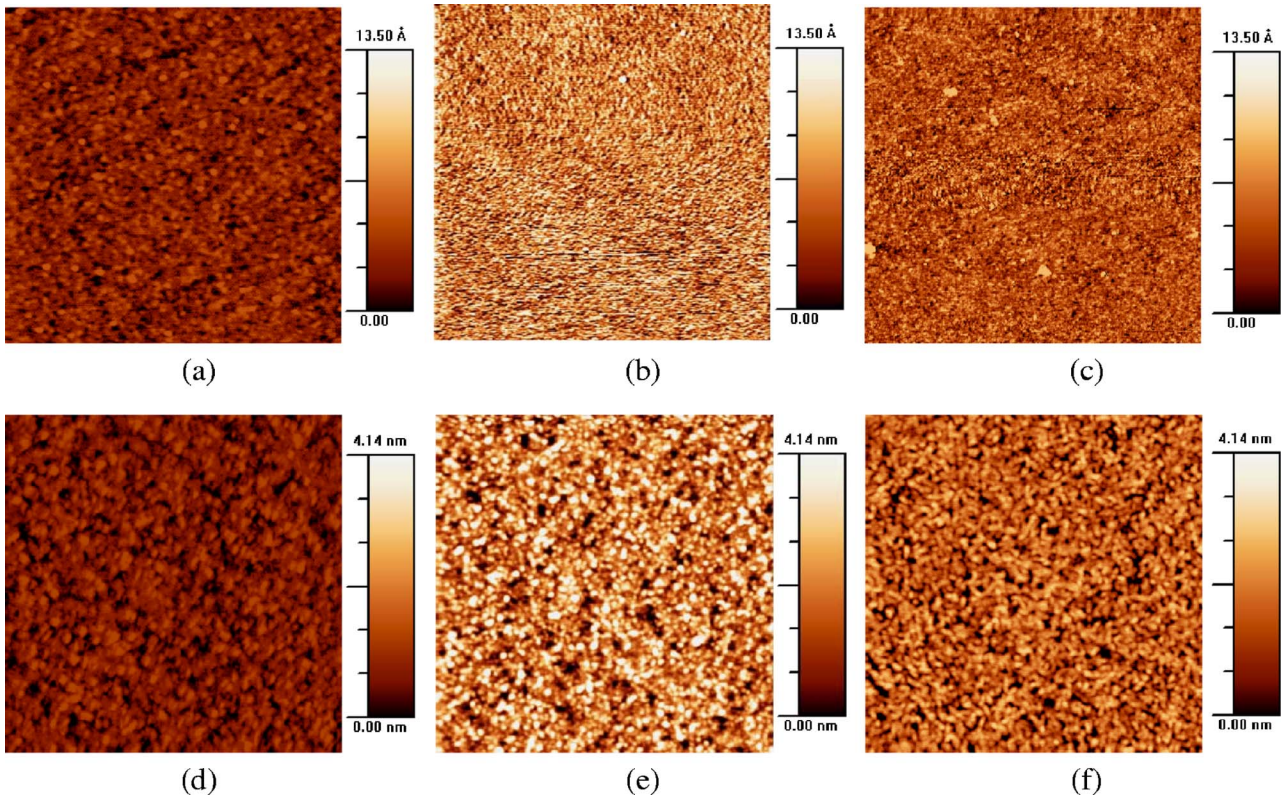

Fig. 2 2×2 μm^2 AFM scans of ML1 and Mo samples before and after exposure in the LPP and DPP source, respectively. (a) Pre-exposed ML1 sample; (b) LPP-exposed ML1 sample; (c) DPP-exposed ML1 sample; (d) pre-exposed Mo sample; (e) LPP-exposed Mo sample; (f) DPP-exposed Mo sample.

LPP exposure was operated at 500,000 shots, 20 times fewer than DPP exposure at 10 million shots. Moreover, the LPP exposure time of ~5 min, i.e., the interaction of mirror surfaces with the plasma environment, is much less than DPP exposure of ~11 h. This difference is expected to be compensated for somewhat by the samples being much closer to the LPP source (10 to 17 cm versus 56 cm) and the lack of debris mitigation on the LPP source.

3 Results and Discussion

3.1 *Surface Roughness*

Surface roughness can limit reflectivity of surfaces, particularly in the case of a grazing incidence collector. To investigate how the exposures affected the samples in this regard, AFM is used to measure surface height variations over several different lateral length scales. Scans are done over $5\times5, 2\times2, 1\times1$, and 0.5×0.5 μm^2 areas. Examples shown in Fig. 2(a)–2(f) are 2×2 μm^2 AFM scans of MLl and Mo of the seven samples before and after exposure in the LPP and DPP source, respectively.

All samples except the ML1 and LPP-exposed C sample show a clear increase in visual roughness. When analyzed by computer, the RMS roughness is calculated, which is the most commonly quoted roughness parameter.[15] Table 1 summarizes the AFM results, giving the calculated RMS roughness values for each of the seven samples. In all but one case, the roughness values increased by a factor of between 1.1 and 6.1 times. The metallic films Au, Mo, Pd, and Ru showed the most dramatic increases in roughness, followed by Si and C. The multilayer mirror actually became slightly smoother after exposure, which is perhaps an unexpected result. It is possible that if the top Ru surface that is relatively rough were eroded, the underlying Si layer would be significantly smoother. This hypothesis is supported by the erosion measurements presented in Sec. 3.3.

XRR measurements give information on film thickness, interfaces, and roughness by measuring the intensity of reflected x-rays versus angle. Interfaces show up as interfer-

Table 1 AFM results for pre-exposed, LPP-exposed (no debris mitigation), and DPP-exposed samples. The RMS roughness is in units of nm.

Sample	Pre-exp.	LPP-exp.	Change (Exp/pre)	DPP-exp.	Change (Exp/pre)
Au	0.49	2.22	4.5	1.55	3.2
C	0.14	0.16	1.1	0.86	6.1
Mo	0.33	1.04	3.2	0.76	2.3
Pd	0.63	1.07	1.7	1.28	2.0
Ru	0.27	0.58	2.1	0.80	3.0
Si	0.09	0.16	1.8	0.26	2.9
ML1	0.32	0.35	1.1	0.22	0.7

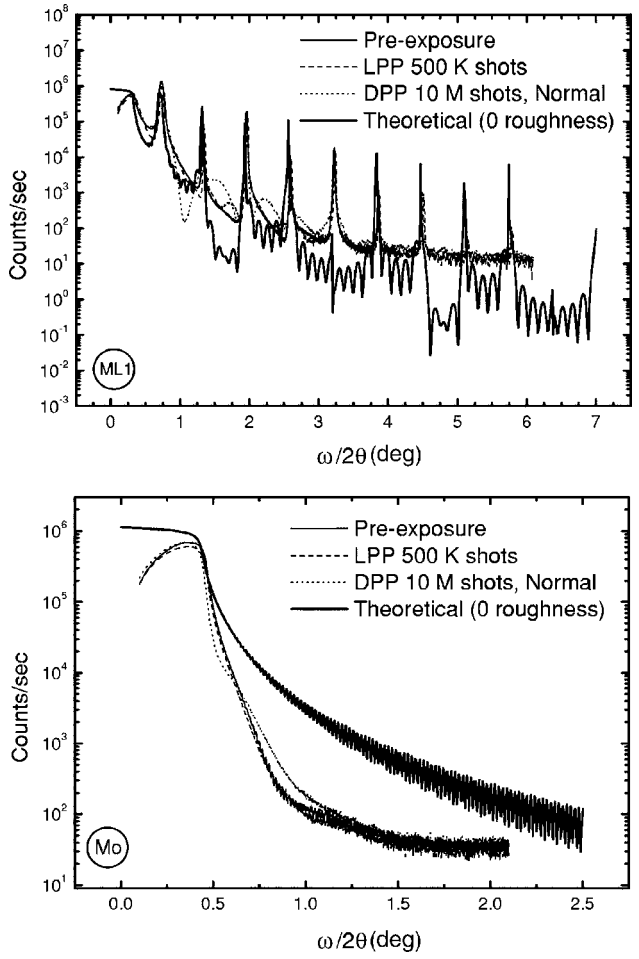

Fig. 3 XRR data and theoretical curve for ML1 and Mo, respectively.

ence patterns in the trace of reflectivity versus angle. Layer thickness is deduced from the period in peaks due to interference off material interfaces. The roughness is determined from the fall off of reflectivity beyond the critical angle. Theoretically, reflectivity should fall off as θ^{-4} according to the Fresnel equation. A faster falloff indicates surface roughness. Because this is an indirect measurement of roughness based on fitting data to a model, it is not as good a measurement as the AFM results shown in Table 1. However, XRR does confirm some of the trends. For example, Au, Mo, Pd, and Ru are definitely more rough than Si and C. The DPP-exposed surfaces also appear to be rougher than their LPP counterparts. Figure 3 details the XRR data for ML1 and Mo. The roughness values obtained by fitting the XRR data to theory are shown in Table 2. It is not clear whether the LPP-exposed samples are rougher than the unexposed samples. However, they are clearly not as rough as the DPP-exposed samples.

3.2 *Sample Texture*

Measurements of the preferred orientation of crystallites, or texture, of the samples are made using XRD. Several different types of scans were performed. A θ to 2θ scan uses a symmetrical geometry where the angle between the surface plane and x-ray source (ω) is equal to the angle between the surface plane and the x-ray detector (θ). A scan over a range of angles with ω and θ coupled while recording the diffracted intensity gives the overall crystallinity of the sample as well as the out-of-plane lattice spacing. The intensity peaks in the out-of-plane lattice spacing show which crystal orientations are present in the sample. Examples of the θ to 2θ scans are shown in Fig. 4(a)–4(f) for ML1 and Mo. In all cases, the films are grown on a (100) Si substrate, so no other peaks could be seen around the dominant peak from the substrate between 60 and 70 deg. This also made it impossible to learn much from the Si film. The C film did not show any peaks in the θ to 2θ scan. This means that the C film is either too thin or amorphous. In the cases that did give good data, all samples showed a strong preference for one orientation as evidenced by relative peak heights significantly different than would be expected in an untextured sample of the same material. Au, Mo, Pd, and Ru favored the (111), (110), (111), and (002) orientations, respectively. These results are summarized in Table 3.

Table 2 XRR results for pre-exposed, LPP-exposed, and DPP-exposed samples.

Sample	Pre-exp.	LPP-exp.	Change (Exp/Pre)	DPP-exp.	Change (Exp/Pre)
Au	1.11	0.99	0.9	1.79	1.6
C	0.79	0.33	0.4	9.20	11.6
Mo	1.70	1.43	0.8	2.00	1.2
Pd	1.26	0.82	0.7	1.14	0.9
Ru	0.31	0.74	2.4	0.98	3.2
Si	0.001	0.001	1.0	—	—
ML1	0.25	—	—	0.15	0.6

A rocking curve can show how strongly orientations are preferred. This is a scan where ω is varied with a fixed 2θ angle. The intensity curve forms a Gaussian peak, with the broadness of the peak giving an indication of the overall crystalline quality of the film and how strongly the orientation is preferred. For example, a single crystal film has a very narrow peak, because as soon as the ω angle is moved the smallest amount, the condition for reflection is broken. Conversely, for completely random orientations (no preference for any orientation over the others), as ω is varied, there is always the same number of crystallites able to reflect the x rays—resulting in a flat rocking curve. Rocking curves are performed on the dominant peak in each sample's θ to 2θ scan. The results are also shown in Table 3.

The broadness of the peaks in the θ to 2θ scan gives the grain size in the direction normal to the surface by measuring the full width at half maximum (FWHM) of the peak and using the Scherrer equation. The results are shown in Table 4 for samples that had well-defined peaks in the θ to 2θ scans. The grain size generally decreases after exposure, and the decrease in the LPP exposures is more pronounced than in the DPP exposures. This is consistent with a higher fluence of damaging ions over the DPP exposures.

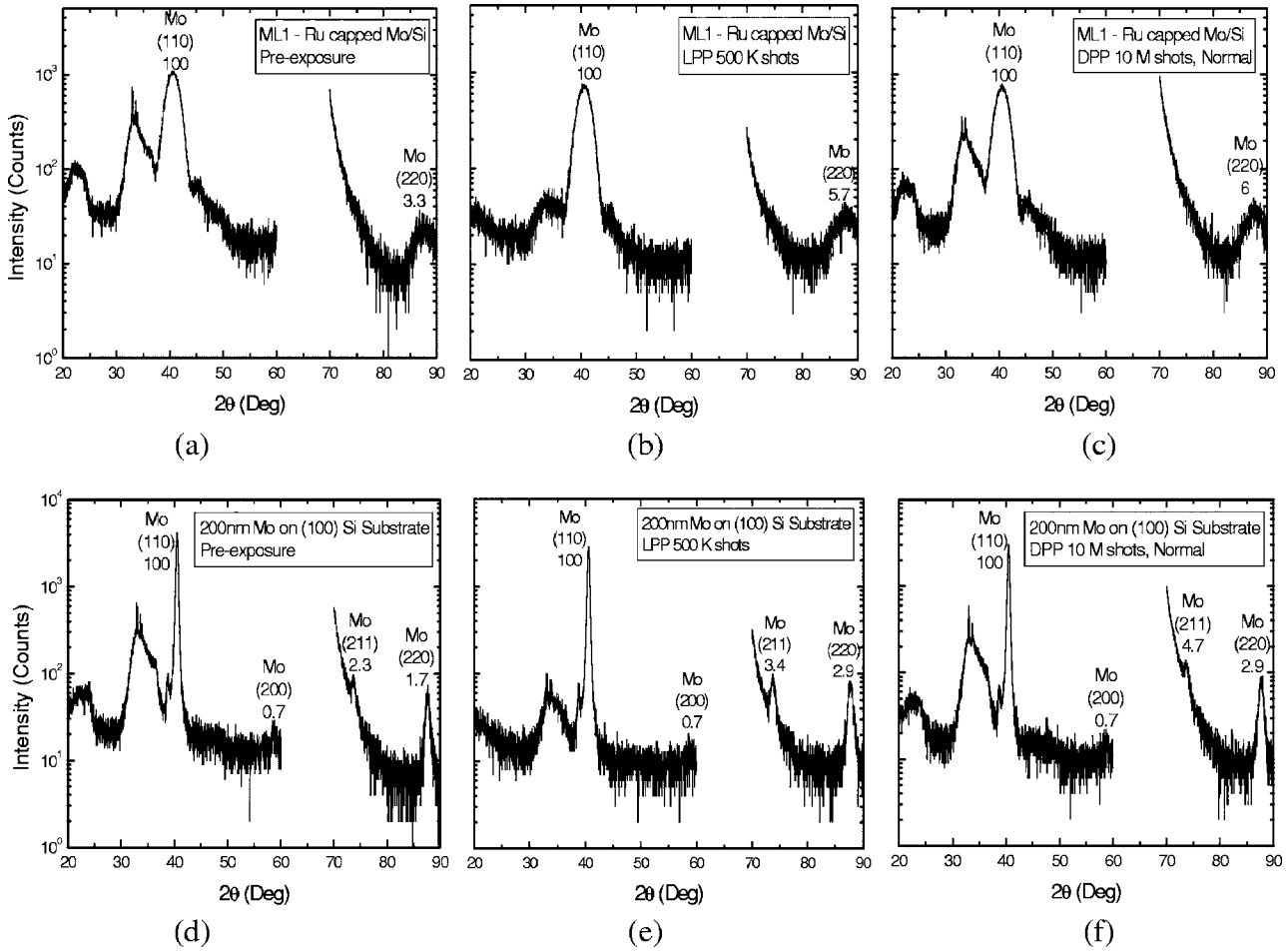

Fig. 4 θ to 2θ scans of ML1 and Mo samples before and after exposure in the LPP and DPP source, respectively, (a) Pre-exposed ML1 sample; (b) LPP-exposed ML1 sample; (c) DPP-exposed ML1 sample; (d) pre-exposed Mo sample; (e) LPP-exposed Mo sample; (f) DPP-exposed Mo sample.

A pole figure is a texture measurement done by rotating the sample about its surface normal (φ) and tilting the sample about its axis parallel to the direction of the x rays (ψ). The source (ω) and detector (θ) angles are fixed to look at a particular orientation of planes. Pole figures can give the preferred orientation and indicate whether the sample is single- or poly-crystalline. Most of the metallic films exhibited a fiber texture, with many grains favoring a particular orientation but all with different rotations in the plane of the sample. These films grow in columns extending vertically up from the substrate. A columnar structure like this can affect the diffusion and transport of particles in the film, for example, resulting in the impact on the collector reflectivity.[16] Diffusion is much faster in the direction normal to the surface (along the grain boundary) than in a direction parallel to the surface in these samples.

As an example of the fiber texture, Fig. 5 clearly shows that the LPP-exposed Au sample exhibits a fiber texture favoring the (111) direction. The (111) orientation is seen as a strong peak in the center of the (111) pole figure. The (111) direction is also seen in the (200) pole figure as the ring positioned 54 deg out from the center (in the ψ direction). The fact that the ring is uniform as the sample is rotated in the ω direction shows that it is not a single crystal. A single crystal would show four discrete peaks separated by 90 deg in φ rather than a ring. A perfect example of a single crystal is shown in Fig. 6 for Si. Here the preferred (100) direction appears as four discrete peaks separated by 90 deg in the (220) pole figure. This suggests that the Si film grown on the Si substrate is either too thin and the signal is dominated by the substrate in these XRD measurements, or that it grew epitaxially. The latter is more likely, since the film should be ~200-nm thick.

In summary, metallic films exhibit a fiber texture, tending to grow up from the substrate in vertical columns. The multilayer, C, and Si films are harder to evaluate. Individual layers of the multilayer are extremely thin, and the Si layers match the substrate. The Si film is likely single crystal, like the substrate. The C film is either too thin to measure well or amorphous. There is some decrease in average grain size after exposure, but XRD on the LPP-exposed samples shows little change from the pre-exposed or DPP-exposed samples.

3.3 *Erosion*

In theory, thickness estimates are obtained by depth profiles in a technique like AES. If the depth profile is performed by sputtering all the way through the film into the substrate,

Table 3 X-ray diffraction θ to 2θ peaks, normalized to the largest peak that would be found in an untextured sample.

			Normalized peak height				FWHM of rocking curve (deg)		
Sample	2θ (deg)	h k l	Untextured	Pre-exp.	LPP-exp.	DPP-exp.	Pre-exp.	LPP-exp.	DPP-exp.
Au	38.18	1 1 1	100	100.0	100.0	100.0	5.78	5.84	5.68
	44.39	2 0 0	52	0.0	0.0	0.0	—	—	—
	77.54	3 1 1	36	0.1	0.1	0.2	—	—	—
	81.72	2 2 2	12	2.4	3.9	4.4	—	—	—
Mo	40.55	1 1 0	100	100.0	100.0	100.0	12.3	12.5	13.0
	58.66	2 0 0	16	0.7	0.7	0.7	—	—	—
	73.75	2 1 1	31	2.3	3.4	4.7	—	—	—
	87.68	2 2 0	9	1.7	2.9	2.9	—	—	—
Pd	40.11	1 1 1	100	100.0	100.0	100.0	8.44	8.59	8.44
	46.65	2 0 0	60	0.5	0.6	0.7	—	—	—
	82.10	3 1 1	55	0.5	1.0	1.2	—	—	—
	86.61	2 2 2	15	1.5	2.9	2.9	—	—	—
Ru	38.42	1 0 0	40	29.0	30.1	28.0	—	—	—
	42.18	0 0 2	35	797.0	806.8	826.0	9.53	9.46	9.63
	44.04	1 0 1	100	100.0	100.0	100.0	—	—	—
	78.46	1 0 3	25	2.0	3.3	4.2	—	—	—
	82.30	2 0 0	6	0.0	0.0	0.0	—	—	—
	84.79	1 1 2	25	2.5	5.1	5.5	—	—	—
	86.04	2 0 1	20	3.7	7.5	7.4	—	—	—
Mo in ML1	40.55	1 1 0	100	100.0	100.0	100.0	13.1	13.3	13.3
	58.66	2 0 0	16	0.0	0.0	0.0	—	—	—
	73.75	2 1 1	31	0.0	0.0	0.0	—	—	—
	87.68	2 2 0	9	3.3	5.7	6.0	—	—	—

the amount of sputtering required to reach the substrate gives the film thickness. In practice, however, the sputtering rate is found to vary too much in the AES instrument, and such thickness estimates are not reliable. For the multilayer mirror, however, AES is able to confirm that there are 50 Si and Mo layers (Fig. 7).

The best measurements of thickness that we obtained were from cross-sectional SEM. Figure 8(a)–8(f) shows film cross sections for two of the samples before and after exposure in the LPP and DPP source, respectively. Table 5 summarizes the thickness measurements derived from the cross sections. When compared to thickness estimates made on the pre-exposed samples, erosion by LPP exposure of between 5 and 48 nm is seen. This is generally less than the erosion seen in the DPP exposures (except for Pd), which is logical because the number of shots is 20 times less in the LPP exposures.

There are issues with measuring a number of samples. The measurement of the Ru sample before exposure is questionable because the film seems to have delaminated in the cross-sectional view. The C and Si samples often do not provide enough contrast to clearly identify the film-

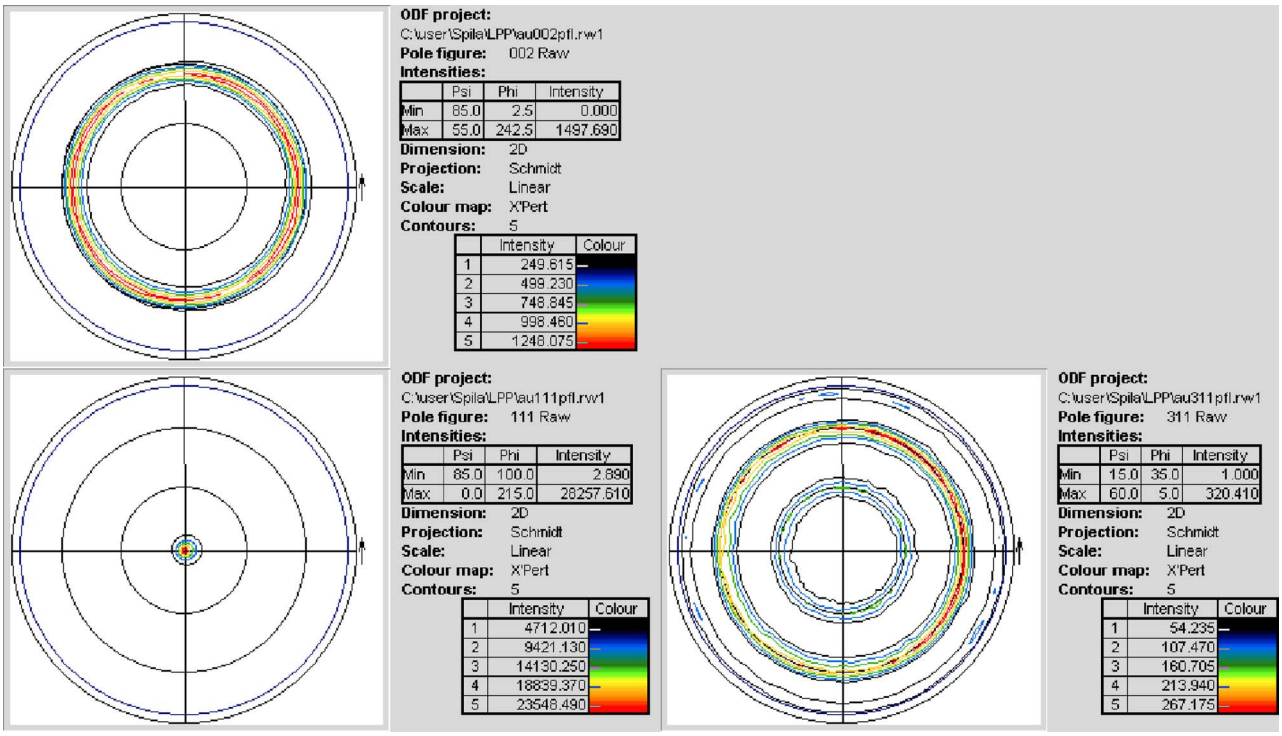

Fig. 5 (002), (111), and (311) pole figures for the LPP-exposed Au sample (color online only).

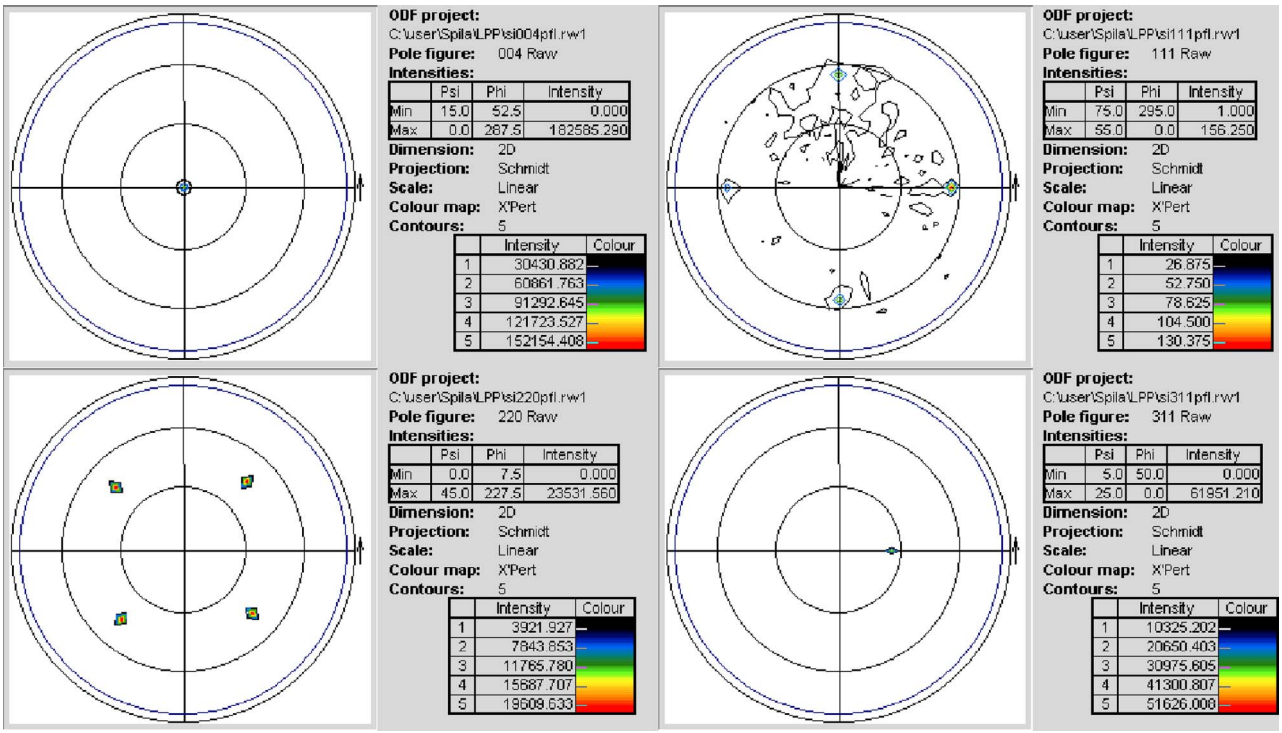

Fig. 6 (004), (220), (111), and (311) pole figures for the LPP-exposed Si sample (color online only).

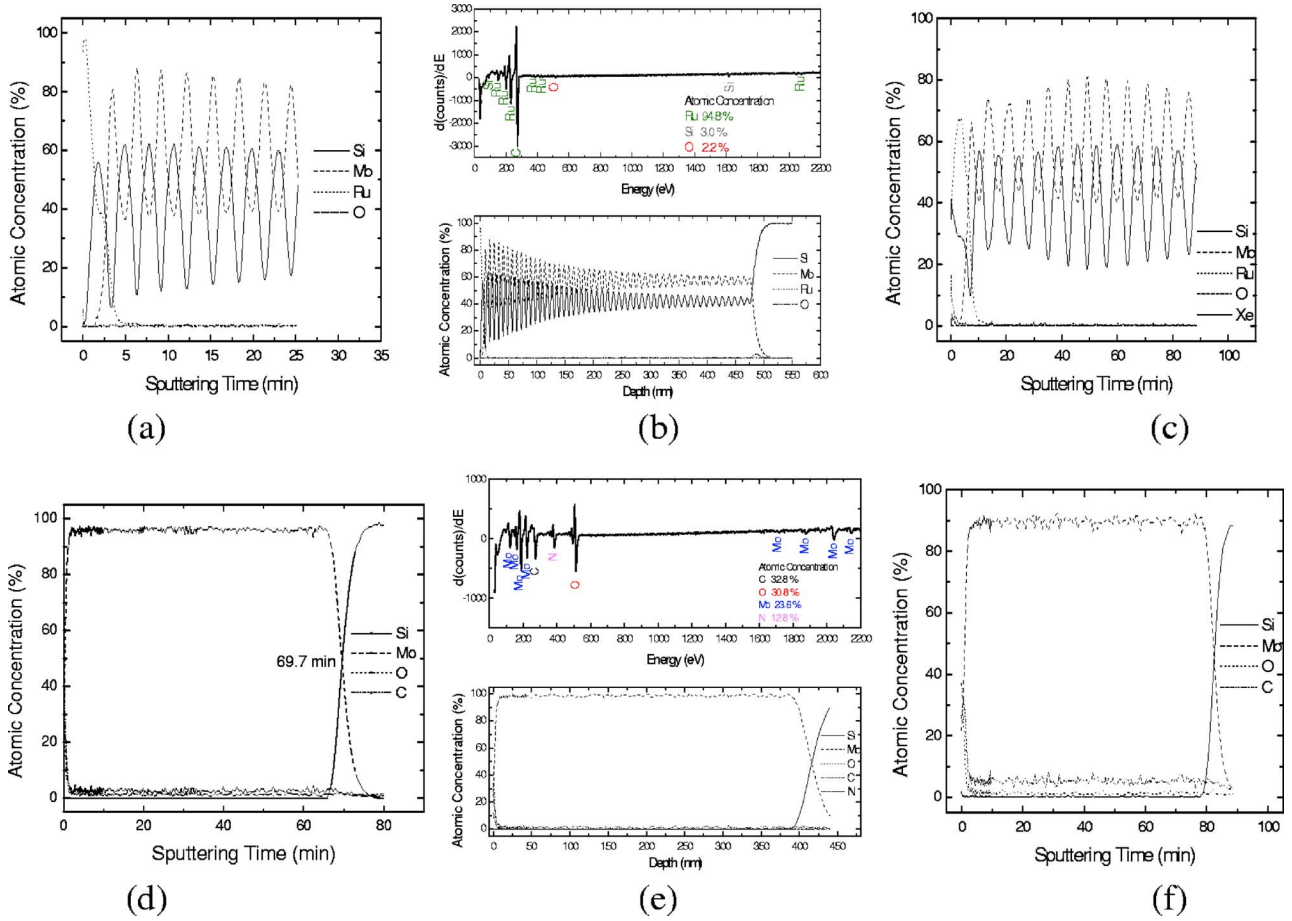

Fig. 7 AES data for the pre-exposed, LPP-exposed, and DPP-exposed ML1 and Mo samples, respectively. (a) Pre-exposed ML1 sample; (b) LPP-exposed ML1 sample; (c) DPP-exposed ML1 sample; (d) pre-exposed Mo sample; (e) LPP-exposed Mo sample; (f) DPP-exposed Mo sample.

substrate. A good C cross section is shown for the LPP-exposed sample, but comparable results from the pre-exposed or DPP-exposed batches were not obtained.

There are several possible reasons for differences in erosion depths between the LPP and DPP exposures. The LPP samples are exposed to 500,000 shots versus 10 million shots for the DPP exposures. However, there is clearly not 20 times less erosion seen in the LPP samples. This indicates that the erosive ion flux on the samples exposed to the LPP source is much higher than the flux on the samples exposed to the DPP source. It is possible that some of this is due to the difference between LPP and DPP sources. However, certainly some of it is attributable to the distance from the source to the samples. The samples were only 10 to 17 cm from the source in the LPP exposures but were 56 cm from the pinch in the DPP exposures. Another major contribution to erosion differences is debris mitigation present in the DPP source but absent in the LPP source.

Table 4 Grain size calculations for Au, Mo, Pd, and Ru samples.

			Grain Size (nm)		
Sample	2θ (deg)	h k l	Pre-exp.	LPP-exp.	DPP-exp.
Au	38.185	1 1 1	351	316	367
Mo	40.550	1 1 0	243	228	241
Pd	40.119	1 1 1	368	334	352
Ru	42.189	0 0 2	324	300	317

Characterization of the z-pinch ejecta in the DPP source is performed to explore the erosion mechanism with a spherical sector energy analyzer (ESA) to measure fast ion species and their energy spectra. This is used to evaluate the debris mitigation tool's ability to divert direct fast ion impact and erosion effects on collector optic surfaces. Microanalysis results are compared to the measured direct ion debris field to determine its contribution to total material erosion and the ability of the debris mitigation tool to effect attenuation of fast ion debris. As shown in Fig. 9, Xe^{+} up to Xe^{+4} ions are measured along with Ar^{+} (buffer gas); electrode materials such as W^{+}, Mo^{+}, and Si^{+}; and finally debris tool materials including Fe^{+} and Ni^{+}. Energy spectra for these species from 0.5 keV up to 13 keV are defined at 20 deg and 30 deg from the pinch centerline in the DPP chamber. Results show creation of high-energy ions and a drop in ion flux with angular increase.[9,10] The dominant

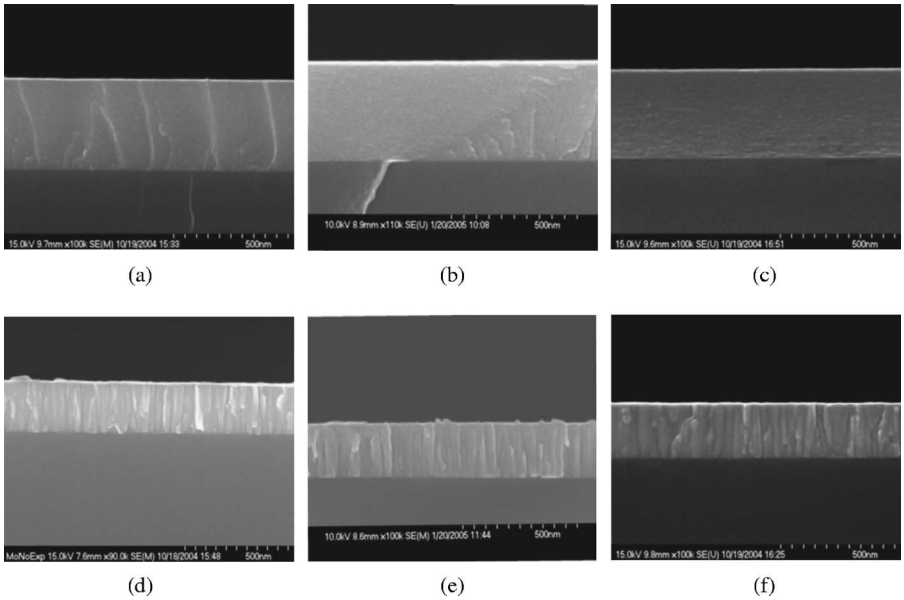

Fig. 8 Cross-sectional SEM images of ML1 and Mo samples before and after exposure in the LPP and DPP source, respectively. (a) Pre-exposed ML1 sample; (b) LPP-exposed ML1 sample; (c) DPP-exposed ML1 sample; (d) pre-exposed Mo sample; (e) LPP-exposed Mo sample; (f) DPP-exposed Mo sample.

specie is Xe^{+},which peaks around ~8 keV, followed by Xe^{2+}, which maximizes at ~5 keV. Ion flux measured against buffer gas flow rate suggests that the direct fast ion population is significantly attenuated through increases in buffer gas flow rate. Data from samples analysis and ESA measurements combined indicate mechanism and effect for debris-optic interactions and detail the effectiveness of the current debris mitigation schemes.[17] The damaging ion flux is attenuated, and the ion energy is decreased by this debris mitigation tool.

3.4 *Composition*

Both AES and XPS are used to investigate the film composition before and after exposure. Both can give the atomic concentration of a sample very near the surface by measuring the kinetic energy of ejected electrons. Some elements are more sensitive to either AES or XPS, warranting use of both techniques. Sputtering through the full sample depth is achievable in AES.

Data shown in Fig. 7(a)–7(f) for AES and Fig. 10(a)–10(f) for XPS show that the LPP-exposed surfaces are mainly free of any contaminants. In contrast, material from the vacuum chamber (e.g., Fe) and from other samples (Au, Mo, Pd, Ru) was redeposited on surfaces in the DPP exposures. Both electrode material and Xe implanted in the samples after DPP exposure, confirming the results from ESA ion debris measurements (see Fig. 9). Some of this is probably due to the fewer number of shots for the LPP exposures. It is also possible that unmeasured Xe exists in the LPP-exposed samples.

Table 6 summarizes notable elements found in the samples, i.e., other than C and O, which are present on all surfaces. In AES, Ar and Si were noted on the C surface before depth profiling would have possibly introduced argon into the sample. Si may have come from other samples or the substrate due to the redeposition of the eroded ma-

Table 5 SEM cross-section thickness measurements for pre-exposed, LPP-exposed, and DPP-exposed samples. Net erosion figures are shown for LPP and DPP exposures for comparison.

	Thickness (nm)			Erosion (nm)	
Sample	Pre-exp.	LPP-exp.	DPP-exp.	LPP erosion	DPP erosion
Au	219	205	165	14	54
C	—	—	—	—	—
Mo	219	211	209	8	10
Pd	278	230	258	48	20
Ru	186	209	200	–23	–14
Si	—	—	—	—	—
ML	355	350	342	5	13

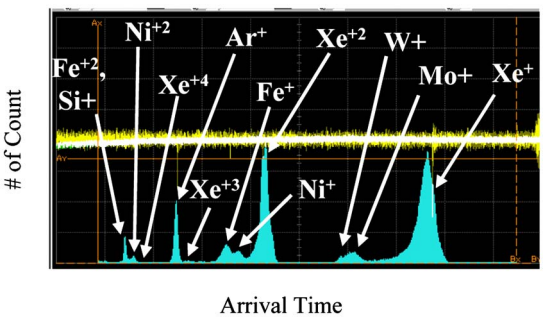

Fig. 9 Oscilloscope image of the ion species peaks discriminated by the ESA-ITOF. Histogram was integrated for 4 min at 256 Hz.

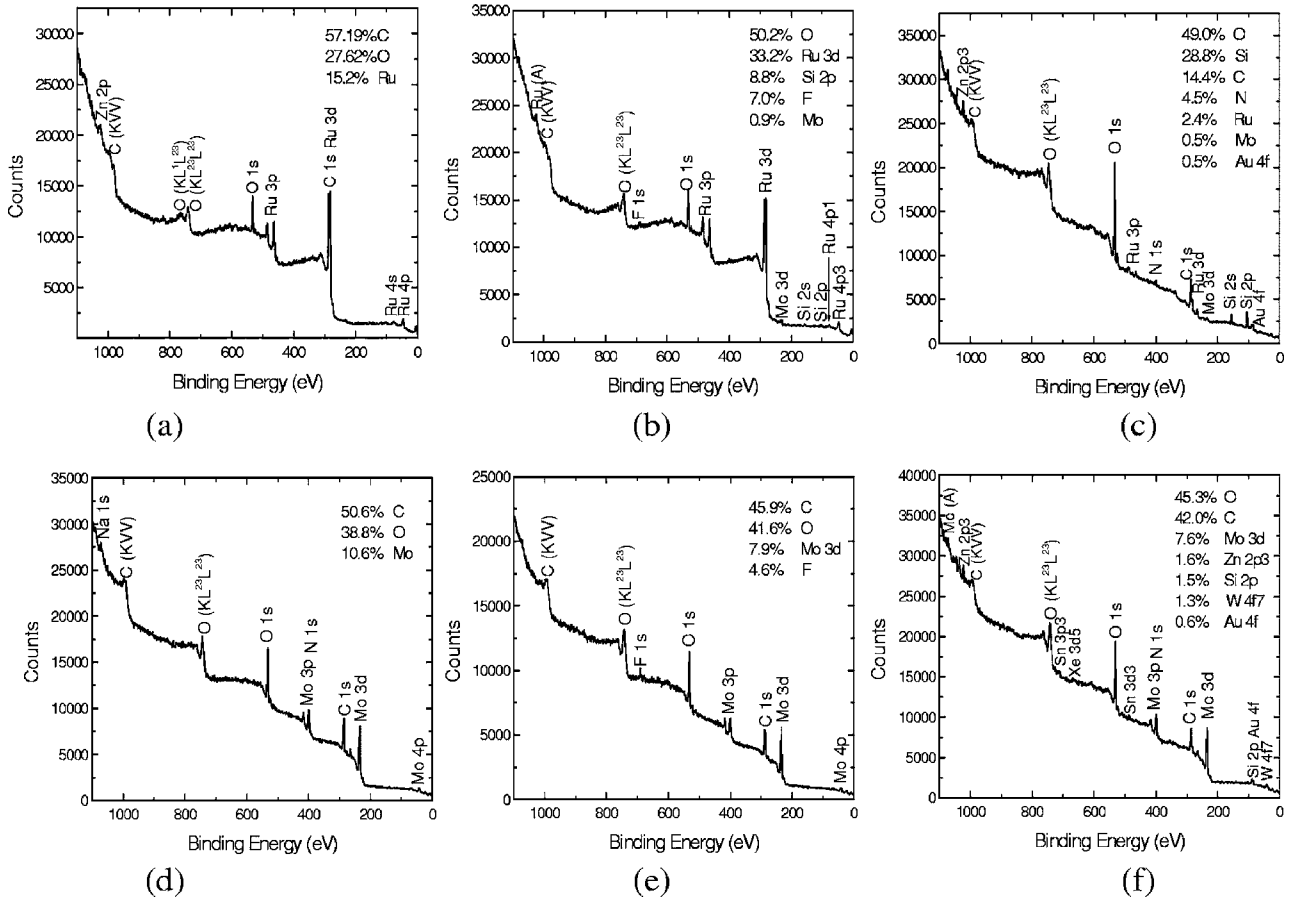

Fig. 10 XPS data for the pre-exposed, LPP-exposed, and DPP-exposed ML1 and Mo samples, respectively. (a) Pre-exposed ML1 sample; (b) LPP-exposed ML1 sample; (c) DPP-exposed ML1 sample; (d) pre-exposed Mo sample; (e) LPP-exposed Mo sample; (f) DPP-exposed Mo sample.

terials during exposures. AES also shows the presence of N on the Mo surface, which is not seen in XPS. XPS shows nitrogen on the LPP-exposed Au surface, as well as possible fluorine. A peak near fluorine's 1s peak appears in the Au, ML1 [Fig. 10(b)], and Mo [Fig. 10(e)] samples. However evidence of F is not seen in AES (which is reasonably sensitive), making its presence questionable. In addition, both AES and XPS show traces of C and S on the Pd sample.

Table 6 Elements seen in AES and XPS.

	LPP-exp.		DPP-exp.	
Sample	AES	XPS	AES	XPS
Au		F,N	Xe	Na
C	Ar, Si	—	Xe, Si, N, Fe	Si, N, Ru, Pd, Mo, Zn
Mo	N	F	Si	Si, W, Au
Pd	Cl,S	Cl, N, S	Cl, N, Si, S	Cl, Zn, Au, S
Ru			Si	Zn
Si				N
ML1		F	Xe	Si, N, Zn

4 Conclusions

Seven samples (Au, C, Mo, Pd, Ru, Si, and ML1) exposed in the ETS LPP source at SNLL and the XTS DPP source at UIUC are analyzed at the University of Illinois. Samples are exposed to 500,000 shots in ETS LPP source, which is 20 times fewer than the initial exposures performed in the XTS DPP source at UIUC. This difference is partially made up by sample proximity to the source in the LPP exposures (10 to 17 cm versus 56 cm in the DPP exposures) and lack of debris mitigation on the LPP source. Analysis of the LPP-exposed samples, as well as earlier analysis of pre-exposed samples and a batch exposed in the DPP source, was performed at the UIUC Center for Microanalysis of Materials. Techniques performed included AFM, XRD, XRR, SEM, AES, and XPS. AFM and XRR give the surface roughness. XRD gives information about the texture of the samples. SEM provides the best estimates of film thickness and erosion. Finally, AES and XPS measure the elemental composition of the samples versus depth.

Six of the seven samples became rougher after exposure in the LPP source. All the samples except one became

rougher in the DPP source. The increase is between 1.1 and 6.1 times. The metallic films (Au, Mo, Pd, Ru) showed the greatest increase in RMS roughness. Carbon after LPP-exposure showed a slight increase in roughness, while the multilayer sample appears smoother after DPP exposure. This can occur if the Ru capping layer is eroded, exposing a smooth Si layer. There is no definite trend in roughness when comparing the LPP and DPP exposures except that roughness generally increases.

In terms of erosion, the LPP samples show less material removed than the DPP exposures. This is partially due to the shorter duration of exposure. The LPP erosion is estimated to be between 5 nm (for ML1) and 48 nm (for Au). In comparison, the DPP erosion varied from 10 nm (for Mo) to 54 nm (for Au). Several samples present measurement problems in cross-sectional SEMs, including C, Si, and Ru. Since the erosion is not 20 times less than in the DPP exposures, it can be concluded that the erosive ion flux to the samples is larger in the LPP exposures. This indicates that fast ion debris mitigation will be needed in LPP sources.

The LPP-exposed samples tend to be "cleaner" than samples exposed in the DPP. In the DPP exposures, various elements are deposited on the sample surfaces (Fe, Au, Ru, Mo, etc.), and some elements (Xe and electrode materials) deposit deep in the surfaces due to energetic impact. Future XPS depth profiling work may determine more conclusively whether debris ions are implanted in the LPP-exposed samples.

The XRR and XRD results indicate changes in grain size, crystallinity, texture, and orientation of the collector optic samples exposed before and after DPP/LPP EUV sources. Metallic films exhibit a fiber texture, tending to grow up from the substrate in vertical columns. There is some decrease in average grain size after exposure, but XRD on the LPP-exposed samples shows little change from the pre-exposed or DPP-exposed samples. All these changes have consequences for the reflectivity degradation of the collector. Columnar grain structure and size may be a concern[18] due to High Spatial Frequency Roughness (HSFR) together with the common RMS roughness, since the grain size is comparable to the EUV wavelength around 13.5 nm.

Acknowledgments

The authors would like to thank project manager Ginger Edwards and to acknowledge support from SEMATECH. Additional assistance from Saša Bajt at Lawrence Livermore National Laboratory, Richard Anderson at Sandia National Laboratory at Livermore, Robert Bristol at Intel Components Research, and the Xtreme Technologies GmbH team in Göttingen was wholeheartedly appreciated. A portion of this research was carried out in the Center for Microanalysis of Materials, University of Illinois, which is partially supported by the U.S. Department of Energy under grant DEFG02-91-ER45439.

References

1. Huatan Qiu et al., "Characterization of collector optic material samples before and after exposure in LPP and DPP EUV sources," *Proc. SPIE* **5751**, 1211–1222 (2005).
2. D. A. Alman et al., "UIUC collector erosion and optical lifetime project results: Time dependent exposures," *Proc. SPIE* **5751**, 1118–1124 (2005).
3. D. A. Alman, H. Qiu, T. Spila, K. C. Thompson, E. L. Antonsen, B. E. Jurczyk, and D. N. Ruzic, "Characterization of collector optic material samples exposed to a DPP EUV light source," (unpublished).
4. Xtreme Technologies GmbH, www.xtremetec.de, Gottingen, Germany.
5. U. Stamm, "Extreme ultraviolet light sources for use in semiconductor lithography—state of the art and future development," *J. Phys. D* **37**, 3244–3253 (2004).
6. R. J. Anderson, D. A. Buchenauer , L. Klebanoff, O. R. Wood II, and N. V. Edwards, "The erosion of materials exposed to a laser-pulsed-plasma (LPP) extreme ultraviolet (EUV) illumination source," *Proc. SPIE* **5374**, 710–719 (2004).
7. R. J. Anderson, D. A. Buchenauer , K. A. Williams, W. M. Clift, L. E. Klebanoff, N. V. Edwards, O. R. Wood II, and S. Wurm, "Investigation of plasma-induced erosion of multilayer condenser optics," *Proc. SPIE* **5751**, 128–139 (2005).
8. U. Stamm et al., "EUV source power and lifetime: The most critical issues for EUV lithography," *Proc. SPIE* **5374**, 133–144 (2004).
9. E. L. Antonson et al., "XCEED: XTREME commercial EUV exposure diagnostic experiment," *Proc. SPIE* **5751**, 1192–1202 (2005).
10. E. L. Antonson, K. C. Thompson, M. R. Hendricks, D. A. Alamn, B. E. Jurczyk, and D. N. Ruzic, "Ion debris characterization from z-pinch extreme ultraviolet light source," *J. Appl. Phys.* **99**, 063301 (2006).
11. K. C. Thompson, E. L. Antonson, M. R. Hendricks, B. E. Jurczyk, M. Williams, and D. N. Ruzic, "Experimental test chamber design for optics exposure testing and debris characterization of a Xenon discharge produced plasma source for extreme ultraviolet lithography," *Microelectron. Eng.* **83**, 476–484 (2006).
12. S. Bajt et al., "Design and performance of capping layers for extreme-ultraviolet multilayer mirrors," *Appl. Opt.* **42**, 5750–5758 (2003).
13. S. Bajt, J. B. Alameda, T. W. Barbee, Jr., W. M. Clift, J. A. Folta, B. Kaufman, and E. A. Spiller, "Improved reflectance and stability of Mo-Si multilayers," *Opt. Eng.* **41**, 1797–1804 (2002).
14. L. A. Shmaenok et al., "Demonstration of a foil trap technique to eliminate laser plasma atomic debris and small particulates," *Proc. SPIE* **3331**, 90–94 (1998).
15. N. Kandaka, T. Kobayashi, T. Komiya, M. Shiraishi, T. Oshino, and K. Murakami, "Measurement of EUV scattering from Mo-Si multilayer mirrors," *3rd EUVL Symposium*, Miyazaki, Japan (2003).
16. J. J. MacFarlane, C. L. Rettig, P. Wang, I. E. Golovkin, and P. R. Woodruff, "Radiation-hydrodynamics, spectral, and atomic physics modeling of laser-produced plasma EUVL light sources," *Proc. SPIE* **5751**, 588–600 (2005).
17. B. E. Jurczyk et al., "The effect of debris on collector optics, its mitigation and repair: Next-step a gaseous Sn EUV DPP source," *Proc. SPIE* **5751**, 572–577 (2005).
18. M. Putero-Vuaroqueaux, H. Faik, and B. Vidal, "A comparative study of the interfacial roughness," *J. Phys. Condens. Matter* **14**, 8955–8968 (2002).

Biographies and photographs of authors not available